Experimental study of firing death in a network of chaotic FitzHugh-Nagumo neurons

Marzena Ciszak,[1,*] Stefano Euzzor,[1] F. Tito Arecchi,[1,2] and Riccardo Meucci[1]
[1]*CNR-Istituto Nazionale di Ottica, Largo E. Fermi 6, 50125 Florence, Italy*
[2]*Department of Physics, University of Florence, Florence, Italy*
(Received 26 July 2012; revised manuscript received 13 November 2012; published 28 February 2013)

The FitzHugh-Nagumo neurons driven by a periodic forcing undergo a period-doubling route to chaos and a transition to mixed-mode oscillations. When coupled, their dynamics tend to be synchronized. We show that the chaotically spiking neurons change their internal dynamics to subthreshold oscillations, the phenomenon referred to as firing death. These dynamical changes are observed below the critical coupling strength at which the transition to full chaotic synchronization occurs. Moreover, we find various dynamical regimes in the subthreshold oscillations, namely, regular, quasiperiodic, and chaotic states. We show numerically that these dynamical states may coexist with large-amplitude spiking regimes and that this coexistence is characterized by riddled basins of attraction. The reported results are obtained for neurons implemented in the electronic circuits as well as for the model equations. Finally, we comment on the possible scenarios where the coupling-induced firing death could play an important role in biological systems.

DOI: 10.1103/PhysRevE.87.022919 PACS number(s): 05.45.Ac, 87.19.lj, 87.19.lm

I. INTRODUCTION

Although real excitable cells, neuronal or cardiac, are complicated nonlinear systems involving a large number of variables, the essential features of their excitable behavior can be captured by a reduced description. Excitable behavior appears near a bifurcation from a stable fixed point to a stable limit cycle. Two examples are the Andronov bifurcation (or saddle-node bifurcation on an invariant circle) [1] and the Hopf bifurcation (or Andronov-Hopf bifurcation) [2]. The simplest representations of excitable dynamics are the phase equation (or Adler system) for the Andronov bifurcation and the FitzHugh-Nagumo (FHN) model [3,4] for the Hopf bifurcation. The FHN model alone exhibits only regular dynamics since it is two dimensional. A chaotic spiking regime can be induced in FHN by introducing a third slow refractory variable [5,6] or by adding a periodic driving [7]. By changing the amplitude or frequency of the external driving the system undergoes period doubling to chaos and transition to chaotic mixed-mode oscillations (MMO's) [8,9]. Mixed-mode oscillations (chaotic subthreshold oscillations interrupted by large spikes) were first discovered in chemical systems (Belousov-Zhabotinsky reaction) [10], and since then they have been frequently observed in other systems, such as biological [11] or optical [12] ones (see Ref. [13] for a recent review).

In the case of spatially extended systems, the dynamical regimes of the single nodes and global states are influenced by the intercellular interactions through the different types of coupling. For example, the chaotic spiking behavior in the two-dimensional oscillatory FHN can be induced by coupling systems in a network [14]. It has been shown that coupling can also induce a quasiperiodic motion [15,16]. The transition from regular periodic dynamics to quasiperiodicity may occur through Neimark-Sacker [17] or border-collision [18] bifurcations. These bifurcations lead to a quasiperiodic route to chaos (Ruelle-Takens scenario). The emergence of complex firing patterns in a neural network may be induced not only by coupling but also by the presence of delays [19]. Despite the dynamical changes and creation of multistable states, above a certain coupling strength, the systems eventually reach full synchronization (see, e.g., Refs. [20,21]).

On the other hand, the coupling may reduce the complexity of the network leading to the so-called *oscillation* or *amplitude death* where the dynamics of each subsystem ends up in a stable fixed point through the Hopf or saddle-node bifurcations.

It was shown in Ref. [22] that in a pair of weakly nonlinear oscillators, the coupling strength causes the system to stop oscillating, and the rest state at zero, stabilized by the interaction, is the only stable solution. The amplitude death may be eliminated by introducing the disorder in the form of random deviations from a linear trend of frequencies in an array of diffusively coupled limit-cycle oscillators [23]. Such an approach weakens considerably desynchronization-induced oscillator death and, as a result, increases oscillation intensity substantially. The amplitude death was also demonstrated to be induced not only by coupling but also by time delay [24]. It was shown in two coupled nonlinear electronic circuits that are individually capable of exhibiting limit-cycle oscillations. Other experimental observations regarded a pair of thermo-optical oscillators linearly coupled by heat transfer [25] and coupled Chua circuits [26]. It was demonstrated in Ref. [25] that the death phenomenon occurs because the coupling displaces the Hopf bifurcation point.

A similar phenomenon takes place in the systems with two time scales. The large coupling may lead to the so-called *firing* or *spike death* in a network, where the coupled neurons enter the subthreshold oscillation regime. It was demonstrated [27–29] that coupling induces deformation of the slow manifolds leading to suppression of large-amplitude oscillations (canards). In Ref. [29], two coupled FHN have been studied theoretically, examining their response to heterogeneous external parametrical inputs applied to the slow variable. The firing death was shown to occur at large coupling strengths and to be caused by a coupling-induced modification of the slow manifold leading to the increase of the excitation threshold.

In this paper, we examine a network of four FHN electronic neurons coupled in a ring configuration subjected

*Corresponding author: marzena.ciszak@ino.it

to homogenous external inputs in the fast variables. We show that the firing death may occur at small coupling strengths, i.e., before the full synchronization establishes. The occurrence of this phenomenon at small coupling strengths is possible because the slow manifold is modified by both the external forcing and coupling. As the coupling strength is slowly increased, the firing is replaced by subthreshold oscillations exhibiting regular, quasiperiodic (through the Neimark-Sacker bifurcation), or chaotic oscillations. We show numerically that the subthreshold oscillations may coexist with the large-amplitude spiking and that their coexistence is characterized by the riddled basins of attraction. Moreover, we show that either for identical or slightly different systems, the network undergoes similar bifurcation sequences at weak coupling, proving that mostly coupling strength is important in determining the networks' dynamical states. On the other hand, at stronger coupling, we observe various dynamical scenarios for the amplification of the differences between the nodes induced by the coupling. Finally, we analyze the correlations between the nodes during the transition to synchronization and discuss their role in inducing the firing death phenomenon.

II. EXPERIMENTAL SETUP AND THE MODEL

The circuit implementing the FHN is made of commercial semiconductor devices. A network of four FHN has been realized on a printed circuit, planned using OrCad. The electronic network consists of a nearest-neighbor closed-loop coupling scheme, as shown in Fig. 1. The scheme for the electronic circuit reproducing each FHN is shown in Fig. 2(a), while that for the coupling implementation is shown in Fig. 2(b). The equations describing each FHN circuit are

$$\dot{X}_i = \frac{1}{R_1 C_1}\left(X_i - X_i^3/3 - Y_i + V_d + \alpha \Delta X_i\right),$$
$$\dot{Y}_i = \frac{1}{R_1 C_2}\left(\frac{R_1}{R_3} V_b - \frac{R_1}{R_2} Y_i + X_i\right), \quad (1)$$

where $i = 1, \ldots, 4$ indicates the nodes in the network, V_d is the driving signal $A \sin(2\pi \nu t)$, and V_b is a bias voltage. The constant parameters are $R_1 C_1 = 1, C_1/C_2 = 1/(R_1 C_2) = 0.08$, $R_1/R_2 = 0.8$, and $R_1/R_3 = 0.7$, where R stands for resistance and C for capacitor. The nonlinearity X^3 is realized by means of analog multipliers. The temporal scales of the systems are controlled by R_1 and C_1 for the X variable and by R_1 and C_2 for the Y variable. The coupling strength $\alpha = R_e/R$ is determined by a suitable value of a variable resistor. The coupling term is composed with differential amplifiers which allow the subtraction of the signals coming from the neighboring nodes X_{i-1} and X_{i+1} and the feedback signal X_i. ΔX_i is defined as follows:

$$\Delta X_i = X_{i-1} + X_{i+1} - 2X_i \quad (2)$$

for $i = 1, \ldots, 4$ with periodic boundary conditions.

On the other side, the model equations for the driven FHN are the following:

$$\dot{x}_i = x_i - x_i^3/3 - y_i + F + \alpha \Delta x_i,$$
$$\dot{y}_i = \gamma(a - b y_i + x_i), \quad (3)$$

where x_i is the fast variable, y_i is the recovery variable, and $F = A \sin(2\pi \nu t)$ is an external driving term with amplitude

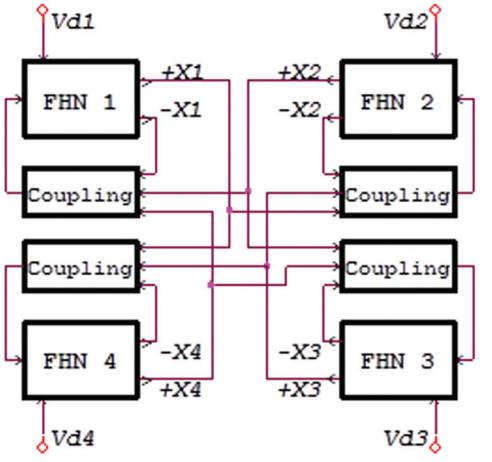

FIG. 1. (Color online) Scheme for the network of four FHN.

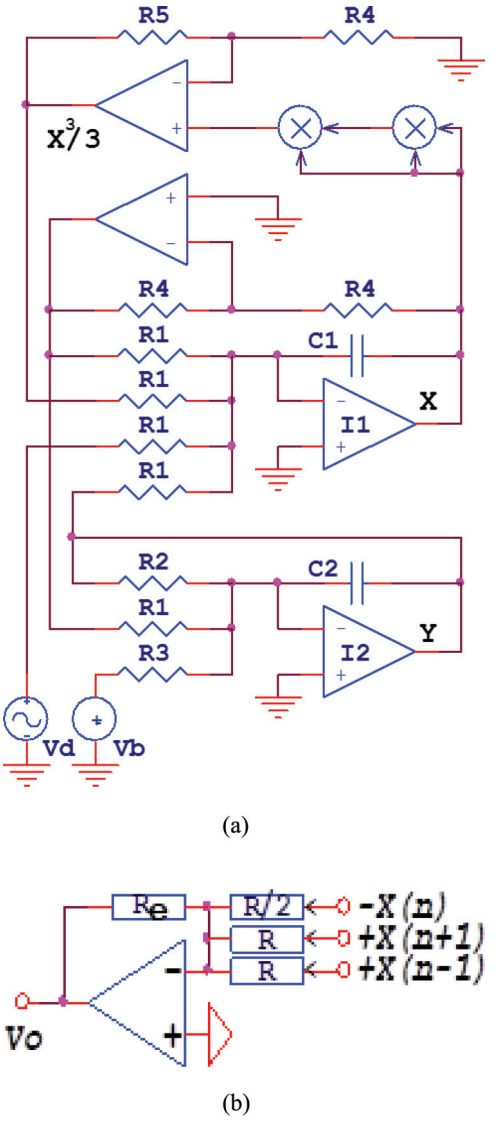

FIG. 2. (Color online) Schemes of (a) the electronic circuit implementing driven FHN and (b) the electronic coupling.

A and frequency $\nu = 1/T$. We consider fixed parameters $\gamma = 0.08, a = 0.7, b = 0.8$, and for the external forcing, $A = 0.485$ and $T = 0.636$. Parameter α is the coupling strength. Equation (3) is transformed to the three-variable set of equations by introducing a new variable $z_i = 2\pi\nu t = \omega t$ as follows:

$$\begin{aligned} \dot{x}_i &= x_i - x_i^3/3 - y_i + A\sin z_i + \alpha\Delta x_i, \\ \dot{y}_i &= \gamma(a - by_i + x_i), \\ \dot{z}_i &= \omega \end{aligned} \tag{4}$$

Δx_i is the coupling term describing the nearest-neighbour configuration:

$$\Delta x_i = (x_{i-1} + x_{i+1} - 2x_i) \tag{5}$$

for $i = 1, \ldots, 4$ and periodic boundary conditions. The model equations have been integrated with fourth-order adaptive step-size Runge-Kutta method.

III. RESULTS

A. Identical vs nonidentical nodes

The experimental implementation of identical oscillators is very hard, and parameter mismatches of unknown magnitude usually arise. A reasonable mismatch in the control parameter can be estimated to be of the order of 10^{-2}. However, in the experimental system we are dealing not only with parameter mismatch but also with an idealized nonlinear function (assumed for simplicity and without loss of generality to be cubic). It is likely that such a mismatch in the description of the nonlinear terms (a multivalued function, though not strictly cubic) is much more relevant than the accuracy in determining the exact values of the control parameters. For the sake of simplicity, here we consider the mismatch only in one control parameter (we choose parameter $a \to a_i$) and find the similar sequences of regimes observed experimentally.

In Figs. 3(a) and 3(b) we plot the bifurcation diagrams in the case of identical model systems for slowly increasing and decreasing coupling strengths, respectively. When the mismatches in the parameters a_i are introduced, the bifurcation diagrams change significantly. By comparing the numerically obtained bifurcation diagrams [Figs. 3(c) and 3(d)] with that obtained experimentally [Figs. 3(g) and 3(h)] we choose the numerical mismatch in the network to be approximately equal to or less than $4 \times 10^{-4}\%$, distributing the mismatches throughout all systems by setting $a_i = 0.7 + 10^{-6}(i-1)$, for $i = 1, \ldots, 4$. The resemblance between numerical and experimental data is quite good and improves at higher coupling strengths. In further study we set this mismatch parameter in the model network. However, it is fair to point out that the numerical mismatch we chose does not correspond to the real mismatches existing in the experiment.

The bifurcation diagrams at weak coupling undergo the same dynamical sequences until approximately $\alpha_c = 8.31 \times 10^{-3}$ for both cases considered, for identical as well as nonidentical systems [see Figs. 4(a) and 4(b)]. Thus, below α_c the network is unsensitive to slight mismatches in the nodes. The situation changes strongly above this critical coupling. As coupling strength is increased ($\alpha > \alpha_c$) the similarity of bifurcation diagrams disappears and each network undergoes various dynamical changes. This fact indicates that above a certain value of the coupling strength the slight differences between the systems start to play an important role in determining the states of the entire network (the mismatches are amplified by coupling). We checked that the network dynamics behave as above until the mismatches in a_i are of the order of 0.4%. We observed that the dynamical structure beyond this limit starts to change throughout all values of α (even below α_c). A similar situation was observed in the case where instead of mismatches in a_i, we drove each system with slightly phase-shifted periodic forcing $\delta\phi \neq 0$, where $\delta\phi = \phi_i - \phi_j$.

In view of the above observations we identify three zones in the coupling strength. The first range below α_c we nominate as the weak coupling zone, the range $\alpha = (\alpha_c, 0.04)$ we nominate as the intermediate coupling zone, and finally, the range above

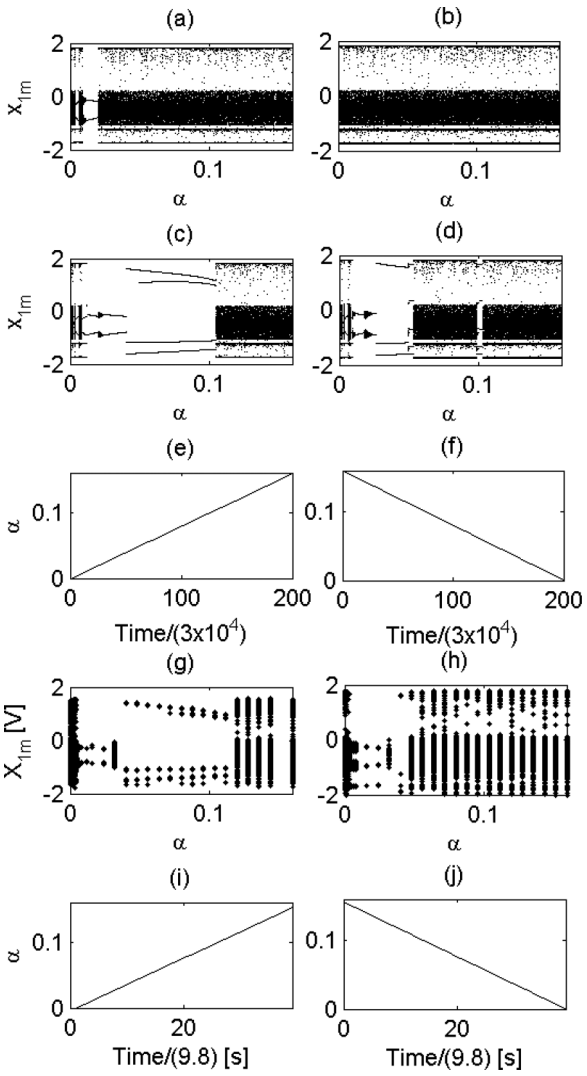

FIG. 3. Bifurcation diagrams for identical model systems with increasing (a) and decreasing (b) coupling, and for the model systems with slight mismatches with increasing (c) and decreasing (d) coupling. The corresponding variations of α in time in the case of a model are shown in (e) and (f). Bifurcation diagrams for the experimental systems with increasing (g) and decreasing (h) coupling. The corresponding variations of α in time in the experiment are shown in (i) and (j).

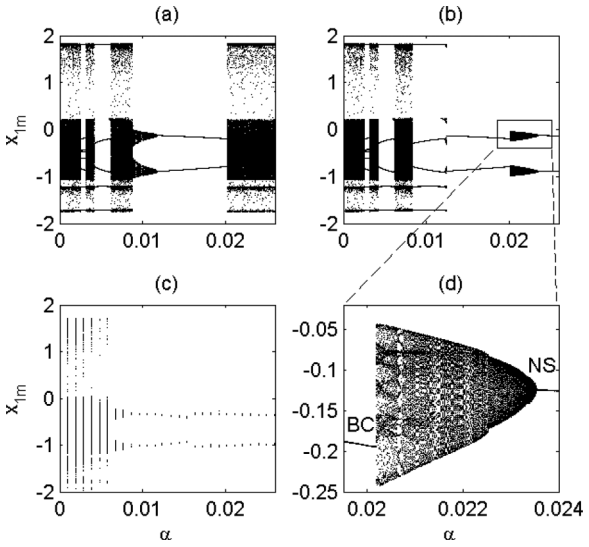

FIG. 4. Zoom of bifurcation diagrams for identical model systems (a), and for model systems with slight mismatches (b) and the experiment (c). In (d) the details of the region with quasiperiodic route to chaos are shown, marking Neimark-Sacker (NS) and boundary crisis (BC) bifurcations. The parameter α is increased as shown in Fig. 3(e).

$\alpha = 0.04$ we nominate as the strong coupling zone. The difference between the intermediate and strong coupling zones is that in the former one the partial or cluster synchronization occurs, depending on the dynamical state of the nodes. On the other side, in the strong coupling zone the full synchronization of chaotic spiking is reached and thus we get the desired synchronization of initial dynamical state (chaotic spiking). It is worth noticing that the dynamical scenarios induced by coupling also differ as the internal parameters of the system are modulated (including the parameters of external forcing).

B. Dynamical regimes induced by coupling

In Figs. 3(c) and 4(b) the bifurcation diagrams show regular MMO's that arise through a boundary crisis, where the chaotic attractor abruptly disappears. In particular, in the range $\alpha = (2.52 \times 10^{-3}, 3.14 \times 10^{-3})$, we identify orbit $L^S = 1^6$, where L stands for large-amplitude spike and S for small-amplitude subthreshold oscillation. Increasing the parameter α, we reach the next window with regular MMO, this time 1^2 that persists in the range $\alpha = (4.17 \times 10^{-3}, 5.91 \times 10^{-3})$. Then orbit 1^3 emerges in the range $\alpha = (5.91 \times 10^{-3}, 6.12 \times 10^{-3})$ that destabilizes through a period-doubling cascade reaching the chaotic spiking again. Finally, in the wide region $\alpha = (0.04, 0.11)$, we observe the 1^0 state.

In the intermediate coupling zone we observe the region of firing death where the large-amplitude oscillations are suppressed, giving rise to the small-amplitude subthreshold oscillations [see Fig. 4(b)]. The firing death is also observed for identical systems [Fig. 4(a)] as well as for systems with much larger mismatches, demonstrating that this dynamical transition is due to the coupling and not the system's diversities.

The presence of the external forcing in the fast variable induces the spike suppression at much smaller coupling strengths compared with the case when it is applied to the slow

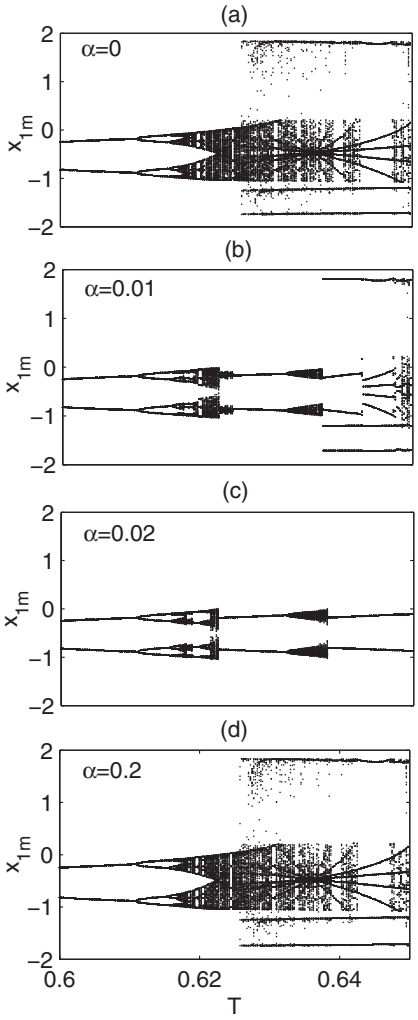

FIG. 5. Bifurcation diagrams for model systems with slight mismatches and modulated period T of external forcing at different magnitudes of the coupling strength: (a) $\alpha = 0$, (b) $\alpha = 0.01$, (c) $\alpha = 0.02$, and (d) $\alpha = 0.2$.

variable. As the coupling strength is increased, the critical point at which the canard explosion takes place is modified. In Fig. 5 we plot the bifurcation diagrams for the system with modulated period T of the external forcing at various magnitudes of the coupling strength α. As α is increased from zero [Fig. 5(a)] to larger values [Figs. 5(b) and 5(c)], we observe the shift toward larger values of T of the transition point at which the canard explosion takes place. Beyond a critical coupling strength, the coupling is no longer effective in the dynamics of the system [see Fig. 5(d)]. This is due to the fact that at large α, when the fully synchronized state is reached, the difference variables Δx_i go to zero (see Sec. III D), and thus after the initial transient the coupling term reaches small values and no longer changes the internal dynamics of the system.

The subthreshold oscillations undergo the transitions from the regular, to quasi-periodic and chaotic. At approximately $\alpha = 0.024$ we observe the Neimark-Sacker bifurcation, where the transition from a periodic to quasiperiodic subthreshold orbit occurs. Successively, the quasiperiodicity route to chaos is observed [see Fig. 4(d)]. Here, this scenario is related with

the change in shape of the subthreshold periodic orbit. At the end of the bifurcation sequence, the chaotic attractor suddenly disappears through a boundary crisis, giving rise to a new periodic orbit. Both orbits, before and after the bifurcation cascade, have the same frequency of oscillations.

The ratio $w = \Omega/\omega$ defines the winding number. It describes the number of times the trajectory winds around the small cross section of the torus (described by Ω, that is the frequency of the system) after going once around the large circumference of torus (described by ω, which is the frequency of driving). If the frequencies are commensurate (w is rational), then the motion is periodic, otherwise (if w is irrational) the trajectory fills the whole toroidal surface and contributes to quasiperiodic motion. At certain coupling values a winding number becomes irrational, which consequently leads to quasiperiodic solutions. In order to detect the quasiperiodic motion we take a Poincaré section of a reconstructed attractor, both experimentally [Figs. 6(a) and 6(b)] and in the model [Fig. 6(c)]. We reconstruct the phase space through the embedding technique with $d = 2$ and take the values of $x(t)$ and $x(t+\tau)$ at times that correspond to a period $T = 2\pi/\omega$ of external forcing. The subthreshold oscillations are composed of subharmonics of order $n = 2$, thus have period $2T$ where T is the period of the fundamental solution (and corresponds to the period of forcing). In the certain range of parameter α each subharmonic undergoes the quasiperiodic route to chaos. As the bifurcation cascade finishes, the subharmonics remain with period $2T$, but change the amplitude of oscillations [see the last panel of Fig. 6(c)].

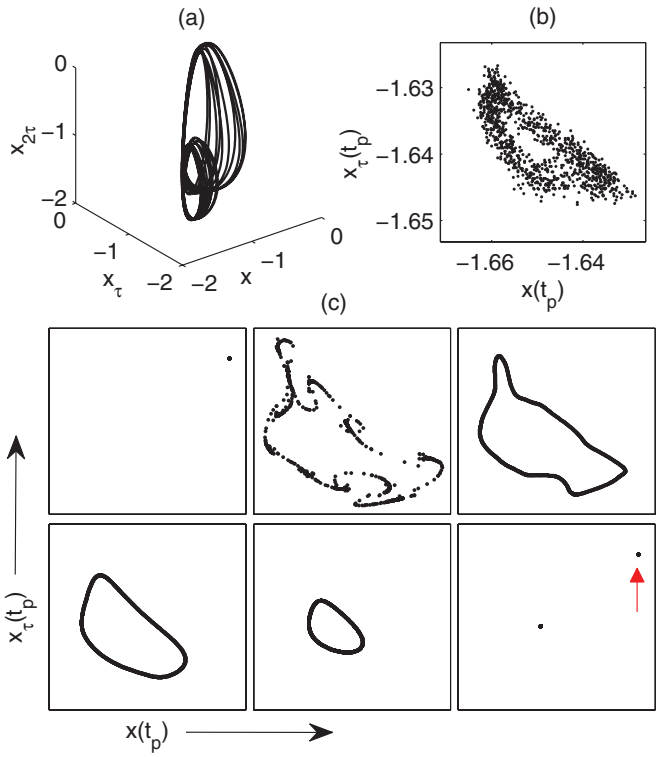

FIG. 6. (a) Reconstructed phase space and (b) corresponding Poincaré cross section obtained from experiment for $\alpha = 0.03$, $A = 899$ mVpp, and $\omega = 400$ Hz. (c) Poincaré cross section in the region where the quasiperiodicity route to chaos is observed. The cross sections are taken for the following coupling parameters: $\alpha = \{0.02, 0.02005, 0.021, 0.0215, 0.023, 0.024\}$. The coupling parameter is increased gradually from 0.02 to 0.024. The small arrow in the last panel marks the orbit before the bifurcation sequence took place (orbit from the first panel).

C. Network multistability

The system exhibits multistable states throughout a wide range of coupling parameters α, well seen as α is slowly increased or decreased (see Fig. 3). We identified various coexistent states including (i) the regular subthreshold oscillations and large-amplitude regular spiking, (ii) regular and chaotic subthreshold oscillations, (iii) various large-amplitude regular spiking, as well as (v) large-amplitude regular and chaotic spiking. Here we analyze in detail only one case (at $\alpha = 0.035$), namely, the coexistence of the regular subthreshold oscillations and spiking.

The basin of attraction of the observed coexistent states exhibits riddling [see Fig. 7(a)]. Riddling refers to the situation in which every point in the basin of attraction of attractor A has pieces of the basin of attraction of attractor B arbitrarily nearby. Thus the existence of riddled basins of attraction compromises the predictability of the final state of the system [30]. The riddled basin can be characterized in terms of the uncertainty exponent γ [31]. We calculate the exponent γ as described in Ref. [32]. First, we choose randomly a phase point r_0. Then we define another phase point $r_0' = r_0 + \delta$, where δ is a small separation from the initial point r_0. Using these two initial conditions we determine whether the final states of the system are different. For a given perturbation δ, we repeat the simulations by choosing randomly many different initial conditions and estimate the fraction M from all realizations N that lead to different states. We fix the initial parameters for three FHN oscillators, while we randomly change those of the remaining one. Using these data, we calculate the probability $P(\delta) = M/N$, and from the assumption that $P(\delta) \sim \delta^\gamma$, we estimate the uncertainty exponent γ. In Fig. 7(b) we plot $\log_{10}(P)$ vs $\log_{10}(\delta)$, with the uncertainty exponent γ that is the slope of the straight line. We have evaluated the system numerically approximately 3.5×10^5 times for each selected δ. Using a linear fit we get the approximate value of the uncertainty exponent to be $\gamma = 0.0053 \pm 3 \times 10^{-4}$, which

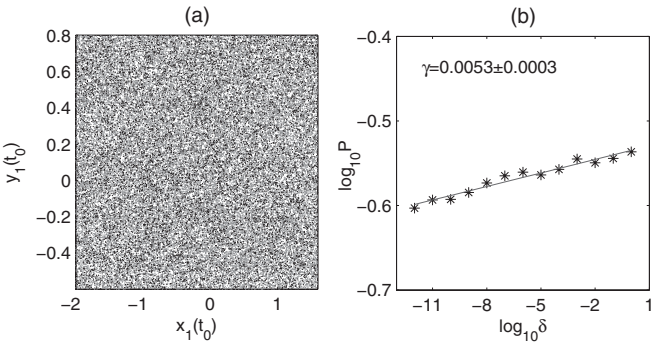

FIG. 7. (a) Basin of attraction for the coupled systems with slight mismatches. Black and gray colors mark small- and large-amplitude oscillations, respectively. (b) The uncertainty exponent calculated for (a).

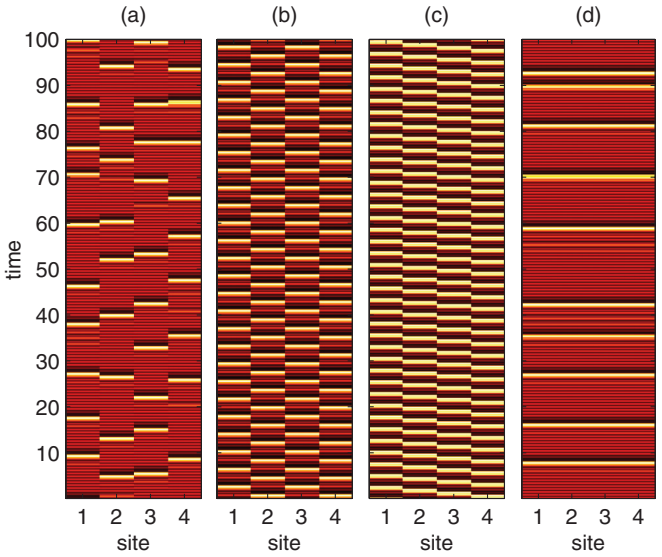

FIG. 8. (Color online) The spatiotemporal patterns observed at different values of the coupling strength α: (a) $\alpha = 0$, (b) $\alpha = 0.0064$, (c) $\alpha = 0.096$, and (d) $\alpha = 0.128$.

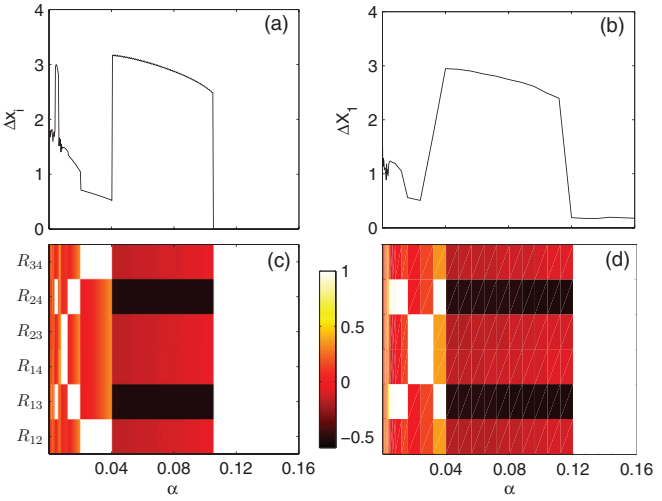

FIG. 9. (Color online) Mean values of the coupling term at one node Δx_1 and ΔX_1 for (a) the model and (b) the experiment, respectively. Correlation coefficient R_{ij} for $i, j = 1, \ldots, 4$ and $i \neq j$ in the case of (c) the model and (d) the experiment.

is considerably smaller than typical values usually obtained for non-riddled basins of attraction. We note that for other coexistent states the basins of attraction also exhibit riddling.

D. Correlation between nodes

In the weak coupling zone the nodes are unsynchronized for $\alpha < 4 \times 10^{-3}$ [Fig. 8(a)] or form two partially synchronized clusters in the range $\alpha = (4 \times 10^{-3}, 8.31 \times 10^{-3})$. As the coupling strength enters the zone of intermediate coupling, the formation of two fully synchronized clusters may be observed if the systems are in the subthreshold regular oscillatory regime [Fig. 8(b)]. Otherwise, if they are quasiperiodic or chaotic, the synchronization is weak or absent. Increasing α, we reach the region $\alpha = (0.04, 0.112)$, where lag synchronization between 1^0 states appears [Fig. 8(c)]. Beyond this region, we enter the strong coupling zone ($\alpha > 0.112$), where fully synchronized chaotic spiking is observed [Fig. 8(d)].

To describe the degree of synchronization between the nodes we use the correlation coefficient $R_{ij} = s_{x_i x_j} / \sqrt{s_{x_i x_i} s_{x_j x_j}}$, where $i, j = 1, \ldots, 4$ and $s_{x_k x_l} = \sum x_k x_l - n \langle x_k \rangle \langle x_l \rangle$ with n standing for the number of data points in the time series. In Fig. 9 we report the mean values of the coupling term at a single node calculated numerically [Fig. 9(a)] and experimentally [Fig. 9(b)] for selected values of parameter α. The coupling term goes to zero as the full synchronization is reached. Before the transition to full synchronization the dynamics of the nodes is differently correlated as can be seen in Figs. 9(c) and 9(d). In the intermediate coupling zone we observe, both numerically and in the experiment, the formation of synchronized clusters. At higher values of coupling, the nodes, being in the regular spiking regime, exhibit lag synchronization that persists in a wide range of α. The interesting behavior is observed during the initial transients in the time series, when the systems are evolved starting from random initial conditions. In the intermediate coupling zone, all transients are in the regime of chaotic spiking (corresponding to the initial state of the network) and are always fully synchronized. However, the final states, beyond the initial transient, being either in the subthreshold oscillatory or regular spiking regime, exhibit only cluster or lag synchronization.

The dynamical regimes that the network has to pass through in order to get synchronized are well visible when the coupling strength is varied slowly and linearly. As the coupling is varied fast to higher values, all dynamical details that we have identified here are lost. The suppression of spiking or emergence of periodic spiking during transition to synchronization at slowly varied coupling strength is an interesting point, suggesting that the coupling strength destroys the initial state completely during the transient, and recovers it through the well-determined bifurcation cascade when full synchronization is reached. This phenomenon may be of crucial importance in biological complex systems, for instance, during the spike timing dependent plasticity (STDP) [33] that controls neural connections, where the synaptic strengths are increased or decreased due to potentiation or depotentiation phenomena, respectively. It could serve as a control tool in the brains' neural network obeying the synaptic plasticity rule and could give rise to fast transitions from quiescence to activity and *vice versa*. In fact, it has been shown that STDP may lead the network to various dynamical states (including chaotic bursting) [34]. Another example to mention is the possible role of the coupling in the emergence of cardiac diseases [35]. The weak coupling between cardiac cells may lead to oscillation death of the given subnetwork and may induce the malfunction of the entire organ.

In the literature, there are several reports on the experimental evidence of the complexity of biological cells, which exhibit various dynamical regimes induced by intercellular chemical or electrical interaction. For example, in Ref. [36] the authors study the network *in vitro* that spontaneously generates an inspiratory-related motor rhythm, also reporting the emergence of MMO's and quasiperiodicity.

IV. CONCLUSIONS

We have shown, both numerically and experimentally, that a slow variation of the coupling in chaotically spiking neurons leads to firing death phenomena where all neurons are set to the subthreshold oscillation state. This occurs below the critical coupling strength at which the full chaotic synchronization is established. The subthreshold oscillations may be regular, quasiperiodic (through Neimark-Sacker bifurcation), or chaotic. Moreover, we have found that these oscillations can coexist with large-amplitude spiking and that this coexistence is characterized by riddled basins of attraction. We have demonstrated that the emergence of firing death at small coupling strength depends strongly on the complexity of a single node, and in particular on the form of the fast variables. We have shown that either for identical or slightly different systems, the coupling strength is most important for determining the networks' dynamical states in the weak coupling zone. On the other hand, in the intermediate and strong coupling zones, differences between the nodes are amplified and various dynamical scenarios emerge, depending on the type of mismatches.

ACKNOWLEDGMENTS

M.C. and R.M. wish to thank Regione Toscana, S. Mancuso, and F. Pavone for financial support. The work was partly supported by Ente Cassa di Risparmio di Firenze.

[1] P. Coullet, T. Frisch, J. M. Gilli, and S. Rica, Chaos **4**, 485 (1994).
[2] E. A. Jackson, *Perspectives of Nonlinear Dynamics*, Vol. 1 (Cambridge University Press, Cambridge, 1989).
[3] R. FitzHugh, Biophys. J. **1**, 445 (1961).
[4] J. S. Nagumo, S. Arimoto, and S. Yoshizawa, Proc. IRE **50**, 2061 (1962).
[5] S. Doi and S. Kumagai, J. Comput. Neurosci. **19**, 325 (2005).
[6] F. Marino, F. Marin, S. Balle, and O. Piro, Phys. Rev. Lett. **98**, 074104 (2007).
[7] E. V. Pankratova, A. V. Polovinkin, and B. Spagnolo, Phys. Lett. A **344**, 43 (2005).
[8] S. Zambrano, I. P. Mariño, J. M. Seoane, M. A. F. Sanjuán, S. Euzzor, A. Geltrude, R. Meucci, and F. T. Arecchi, New J. Phys. **12**, 053040 (2010).
[9] M. Ciszak, S. Euzzor, A. Geltrude, K. Al-Naimee, F. T. Arecchi, and R. Meucci, Cybernetics and Physics **1**, 22 (2012).
[10] V. Petrov, S. K. Scott, and K. Showalter, J. Chem. Phys. **97**, 6191 (1992).
[11] C. Iglesias, C. Meunier, M. Manuel, Y. Timofeeva, N. Delestrée, and D. Zytnicki, J. Neurosci. **31**, 5829 (2011).
[12] F. Marino, M. Ciszak, S. F. Abdalah, K. Al-Naimee, R. Meucci, and F. T. Arecchi, Phys. Rev. E **84**, 047201 (2011).
[13] M. Desroches, J. Guckenheimer, B. Krauskopf, Ch. Kuehn, H. M. Osinga, and M. Wechselberger, SIAM Rev. **54**, 211 (2012).
[14] T. Yanagita, T. Ichinomiya, and Y. Oyama, Phys. Rev. E **72**, 056218 (2005).
[15] M. Sano and Y. Sawada, Phys. Lett. A **97**, 73 (1983).
[16] R. Van Buskirk and C. Jeffries, Phys. Rev. A **31**, 3332 (1985).
[17] I. Gumowski and C. Mira, *Recurrence and Discrete Dynamic Systems*, Lecture Notes in Mathematics, Vol. 809 (Springer, Berlin, 1980).
[18] Z. T. Zhusubaliyeva, E. Mosekildeb, S. Maity, S. Mohanan, and S. Banerjeec, Chaos **16**, 023122 (2006).
[19] O. V. Popovych, S. Yanchuk, and P. A. Tass, Phys. Rev. Lett. **107**, 228102 (2011).
[20] F. Ricci, R. Tonelli, L. Huang, and Y.-C. Lai, Phys. Rev. E **86**, 027201 (2012).
[21] A. Arenas, A. Díaz-Guilera, J. Kurths, Y. Morenob, and C. Zhoug, Phys. Rep. **469**, 93 (2008).
[22] D. G. Aronson, G. B. Ermentrout, and N. Kopell, Physica D **41**, 403 (1990).
[23] L. Rubchinsky and M. Sushchik, Phys. Rev. E **62**, 6440 (2000).
[24] D. V. Ramana Reddy, A. Sen, and G. L. Johnston, Phys. Rev. Lett. **85**, 3381 (2000).
[25] R. Herrero, M. Figueras, J. Rius, F. Pi, and G. Orriols, Phys. Rev. Lett. **84**, 5312 (2000).
[26] I. Gomes Da Silva, S. De Monte, F. d'Ovidio, R. Toral, and C. R. Mirasso, Phys. Rev. E **73**, 036203 (2006).
[27] F. Verhulst and A. Abadi, Z. Angew. Math. Mech. **85**, 122 (2005).
[28] S.-J. Wang, X.-J. Xu, Z.-X. Wu, Z.-G. Huang, and Y.-H. Wang, Phys. Rev. E **78**, 061906 (2008).
[29] D. Hennig and L. Schimansky-Geier, Phys. Rev. E **76**, 026208 (2007).
[30] T. Kapitaniak, Phys. Rev. E **53**, 6555 (1996).
[31] C. Grebogi, S. W. McDonald, E. Ott, and J. A. Yorke, Phys. Lett. A **99**, 415 (1983); S. W. McDonald, C. Grebogi, E. Ott, and J. A. Yorke, Physica D **17**, 125 (1985).
[32] S. Guan, C.-H. Lai, and G. W. Wei, Phys. Rev. E **71**, 036209 (2005).
[33] H. Markram, J. Lubke, M. Frotscher, and B. Sakmann, Science **275**, 213 (1997).
[34] M. Ciszak and M. Bellesi, Chaos **21**, 043119 (2011).
[35] A. Garfinkel, P.-S. Chen, D. O. Walter, H. S. Karagueuzian, B. Kogan, S. J. Evans, M. Karpoukhin, C. Hwang, T. Uchida, M. Gotoh, O. Nwasokwa, P. Sager, and J. N. Weiss, J. Clin. Invest. **99**, 305 (1997).
[36] C. A. Del Negro, C. G. Wilson, R. J. Buter, H. Rigatto, and J. C. Smith, Biophys. J. **82**, 206 (2002).